

Exploring New Biological Functions of Amyloids: Bacteria Cell Agglutination Mediated by Host Protein Aggregation

Marc Torrent^{1,2*}, David Pulido¹, M. Victòria Nogués¹, Ester Boix^{1*}

1 Department of Biochemistry and Molecular Biology, Biosciences Faculty, Universitat Autònoma de Barcelona, Cerdanyola del Vallès, Spain, **2** Department of Experimental and Health Sciences, Universitat Pompeu Fabra, Barcelona Biomedical Research Park, Barcelona, Spain

Abstract

Antimicrobial proteins and peptides (AMPs) are important effectors of the innate immune system that play a vital role in the prevention of infections. Recent advances have highlighted the similarity between AMPs and amyloid proteins. Using the Eosinophil Cationic Protein as a model, we have rationalized the structure-activity relationships between amyloid aggregation and antimicrobial activity. Our results show how protein aggregation can induce bacteria agglutination and cell death. Using confocal and total internal reflection fluorescence microscopy we have tracked the formation *in situ* of protein amyloid-like aggregates at the bacteria surface and on membrane models. In both cases, fibrillar aggregates able to bind to amyloid diagnostic dyes were detected. Additionally, a single point mutation (Ile13 to Ala) can suppress the protein amyloid behavior, abolishing the agglutinating activity and impairing the antimicrobial action. The mutant is also defective in triggering both leakage and lipid vesicle aggregation. We conclude that ECP aggregation at the bacterial surface is essential for its cytotoxicity. Hence, we propose here a new prospective biological function for amyloid-like aggregates with potential biological relevance.

Citation: Torrent M, Pulido D, Nogués MV, Boix E (2012) Exploring New Biological Functions of Amyloids: Bacteria Cell Agglutination Mediated by Host Protein Aggregation. PLoS Pathog 8(11): e1003005. doi:10.1371/journal.ppat.1003005

Editor: H. Steven Seifert, Northwestern University Feinberg School of Medicine, United States of America

Received May 28, 2012; **Accepted** September 17, 2012; **Published** November 1, 2012

Copyright: © 2012 Torrent et al. This is an open-access article distributed under the terms of the Creative Commons Attribution License, which permits unrestricted use, distribution, and reproduction in any medium, provided the original author and source are credited.

Funding: M.T. is a recipient of an Alianza Cuatro Universidades fellowship. D.P. is a recipient of a FPU fellowship (MICINN). Microscopy experiments were carried at the Servei de Microscòpia (UAB) and fluorescence measurements at Servei d'Anàlisi i Fotodocumentació (UAB). The work was funded by MICINN (BFU2009-09371), FEDER funds and Generalitat de Catalunya (2009 SGR 795). The funders had no role in study design, data collection and analysis, decision to publish, or preparation of the manuscript.

Competing Interests: The authors have declared that no competing interests exist.

* E-mail: marc.torrent@uab.cat (MT); ester.boix@uab.cat (EB)

Introduction

Antimicrobial proteins and peptides (AMPs) represent a wide family that contributes to the host defense system with multiple pathogen killing strategies [1–3]. Their fast and multitarget mechanism of action reduces the emergence of bacteria resistance and represents a valuable alternative for common antibiotics [4,5].

The mechanism of action of AMPs has been systematically investigated, suggesting that AMPs bind to bacteria cell membranes and disrupt cell homeostasis. However, more investigations are needed to completely understand how different structures determine the function of AMPs [6–12]. Membrane damage is a multifaceted mechanism that can involve different peptide assemblies and ultimately promotes membrane permeabilization when achieving a critical concentration [13,14]. Several authors have highlighted the striking resemblance of membrane disrupting mechanisms with those observed for amyloid peptides and proteins [15–17]. In both cases, membrane composition (e.g. cholesterol content) and biophysical properties (e.g. membrane fluidity and curvature) were found critical for the peptide action [13,15,18–26]. Furthermore, we have recently suggested that antimicrobial activity could have arisen through cationization of amyloid-prone regions [27]. In this light, some AMPs have been described to form amyloid structures *in vitro* [28,29] and some amyloid peptides have also been considered as putative AMPs [30,31]. In fact, we have

proposed that inherent AMP aggregation properties can modulate antimicrobial activity [32].

Interestingly, some antimicrobial proteins and peptides have been found to agglutinate bacteria cells. In this sense, bacteria agglutination has been ascribed to unspecific adhesion through hydrophobic interactions, as observed for synthetic peptides derived from the parotid secretory protein [33]. Comparative analysis on those peptides highlighted the contributions of both hydrophobic and cationic residues in the agglutination activity [33]. These results suggest that some AMPs could exploit their intrinsic aggregation properties, by triggering bacteria agglutination as part of its mechanism of action as observed for a wealth source of AMPs in saliva, which provides a first barrier to bacteria adherence in the oral cavity [34]. Agglutinating activity has been reported crucial for the antimicrobial function of Eosinophil Cationic Protein (ECP) [35], a small cationic protein specifically secreted by eosinophil granules during inflammation processes with diverse antipathogen activities [36–38]. ECP displays high antimicrobial action, with a specific bacteria agglutination activity reported for Gram-negative bacteria, at a concentration range close to the minimal inhibitory concentration, a behavior that may represent an effective bactericidal mechanism *in vivo* [39].

In order to characterize the relation between AMPs, bacteria agglutination and amyloid aggregation, we have used ECP as a model of study. We present here a detailed characterization of

Author Summary

Microbial infections are reported among the worst human diseases and cause millions of deaths per year over the world. Antibiotics are used to treat infections and have saved more lives than any other drug in human history. However, due to extended use, many strains are becoming refractive to common antibiotics. In this light, new promising compounds, like antimicrobial proteins and peptides (AMPs) are being investigated. Some AMPs also show agglutinating activity; this is the ability to clump bacteria after treatment. This feature is particularly appealing because agglutinating peptides could be used to keep bacteria to the infection focus, helping microbe clearance by host immune cells. In this study, we propose a novel mechanism to explain agglutinating activity at a molecular level using Eosinophil Cationic Protein. We show that the agglutinating mechanism is driven by the protein amyloid-like aggregation at the bacteria cell surface. Accordingly, elimination of the amyloid behavior abolishes both the agglutinating and the antimicrobial activities. This study provides a new concept on how Nature could exploit amyloid-like aggregates to fight bacterial infections. Moreover, these results could also add new insights in understanding the relation between infection and inflammation with dementia and amyloid-related diseases like Alzheimer.

protein-mediated bacteria agglutination and prove the contribution of an aggregation prone domain to the protein antimicrobial action. Complementary studies on model membranes provide a further understanding of the membrane damage process promoted by protein aggregation.

Results/Discussion

ECP was previously reported to aggregate *in vivo* on both bacterial and eukaryotic cell surface without detectable internalization [39,40]. Though these findings were essential to explain the antimicrobial and cytotoxic properties of ECP, the real nature of the aggregation process remained unknown. Besides, the protein has a high affinity towards lipopolysaccharides (LPS) [41] and agglutinates all tested Gram-negative strains [42]. On the other hand, ECP has been reported to form amyloid-like aggregates *in vitro* at specific conditions due to a hydrophobic patch located at the N-terminus. Remarkably, protein amyloid-like aggregation was efficiently abolished by mutating Ile 13 to Ala [28]. The screening of the protein primary structure [43–45] and the design of derived peptides [42,46] also allocated the antimicrobial region at the N-terminus. As the antimicrobial and amyloid active

segments of the protein colocalize [28,35,42,46], it is tempting to hypothesize that bacteria agglutination by ECP could be directly dependent on an amyloid-like aggregation process. This hypothesis raises some exciting questions: (i) Is cell agglutination required for antimicrobial activity? (ii) Is cell agglutination mediated by protein aggregation at the bacteria surface? (iii) Are aggregates formed on the surface of bacteria of amyloid nature?

Bacteria cell agglutination and antimicrobial activities

To address the first question we compared the antimicrobial action of wild type ECP (wtECP) with the I13A mutant, previously described to be unable to form aggregates *in vitro* [28]. The antimicrobial assays reveal that, while wtECP has an average minimal inhibitory concentration (MIC) value around 0.5–1 µM, the I13A mutant is unable to kill bacteria even at 5 µM concentration (Table 1). To further correlate ECP antimicrobial and agglutination activities we studied bacteria cell cultures by confocal microscopy using the SYTO9/Propidium iodide nucleic acid fluorescent labels that allow registering both cell agglutination and viability over time. Interestingly, wtECP can agglutinate Gram-negative bacteria before a viability decrease is observed (Figure 1A), however no cell agglutination takes place when bacteria are incubated with the I13A variant, even after 4 hours (Supporting Information Figure S1). These results are also supported by minimal agglutination concentrations (MAC) close to the MIC values (Table 1) and by FACS experiments showing that wtECP but not I13A mutant is able to agglutinate *E. coli* cells (Figure 1B). Thus, ECP antimicrobial activity on Gram-negative strains is strongly affected when abolishing the agglutination behavior (Ile13 to Ala mutation).

Protein aggregation on membrane models

To further analyze the protein agglutination mechanism, we tested the wtECP and I13A mutant action on a simpler biophysical system such as phospholipid membranes where liposome agglutination is registered as a function of protein concentration. In contrast to wtECP, I13A mutant completely loses the ability to agglutinate membranes (Figure 2A). In particular, when following wtECP agglutinating activity as a function of ionic strength, we observe that liposome agglutination is enhanced at high NaCl concentration (Supporting Information, Figure S2). These results suggest that vesicle agglutination is promoted by hydrophobic interactions. Even more, leakage activity in model membranes is also lost for I13A mutant (Figure 2B), meaning that protein aggregation on the membrane surface is important not only for agglutination but also for later membrane permeabilization. These results are entirely consistent with those described above for bacteria cell cultures where the Ile to Ala mutation not only

Table 1. Antimicrobial (MIC_{100}) and agglutinating (MAC) activities of wtECP and I13A mutant in Gram-negative strains.

	MIC_{100} (µM)		MIC_{100} (µM)		MAC (µM)		MAC (µM)	
	Phosphate buffer ^a		MH medium ^b		Phosphate buffer ^a		MH medium ^b	
	ECP	I13A	ECP	I13A	ECP	I13A	ECP	I13A
<i>E. coli</i>	0.40±0.10	>5	0.45±0.10	>5	0.25±0.1	>5	0.25±0.1	>5
<i>P. aeruginosa</i>	0.60±0.15	>5	0.90±0.20	>5	0.5±0.1	>5	0.5±0.1	>5
<i>A. baumannii</i>	0.75±0.15	>5	1.25±0.20	>5	1.0±0.2	>5	1.0±0.2	>5

^aBacteria were grown in LB medium and incubated with proteins in 10 mM NaH_2PO_4 , 100 mM NaCl pH 7.4.

^bBacteria were grown and incubated with proteins in Mueller-Hinton II broth.

doi:10.1371/journal.ppat.1003005.t001

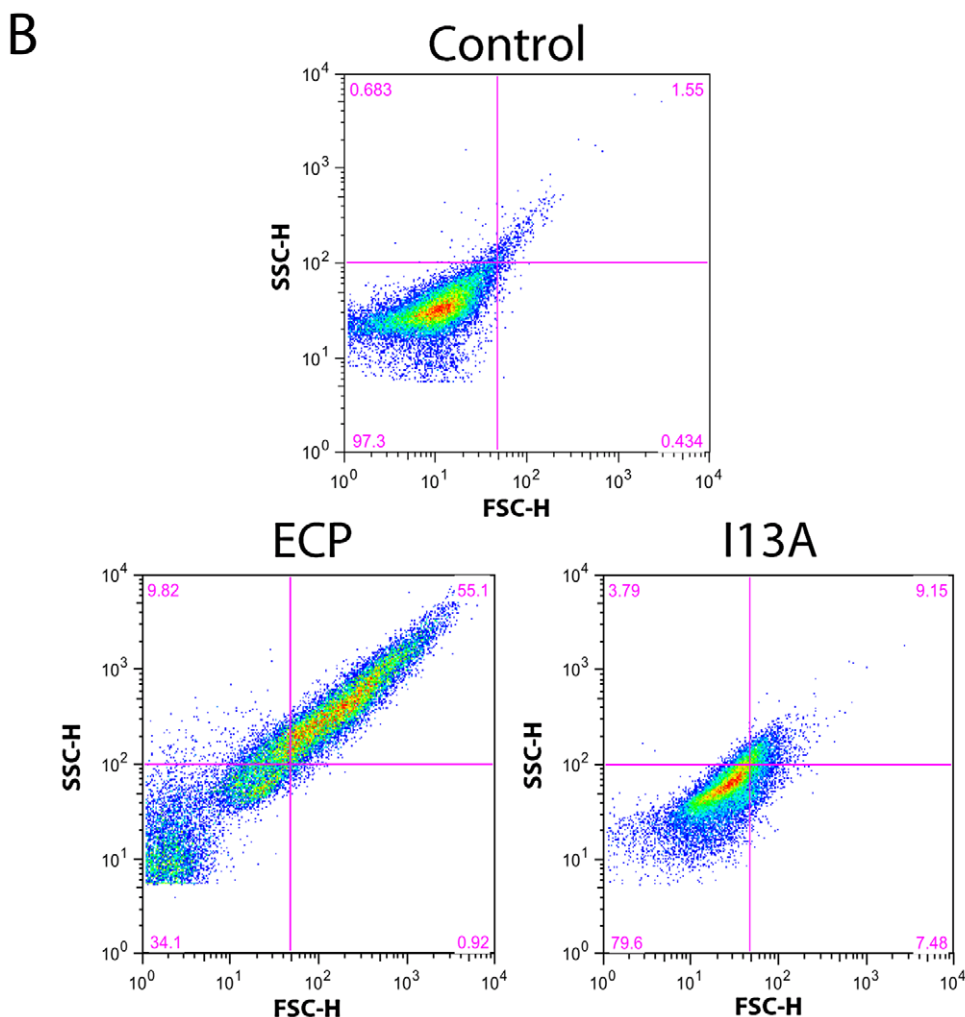
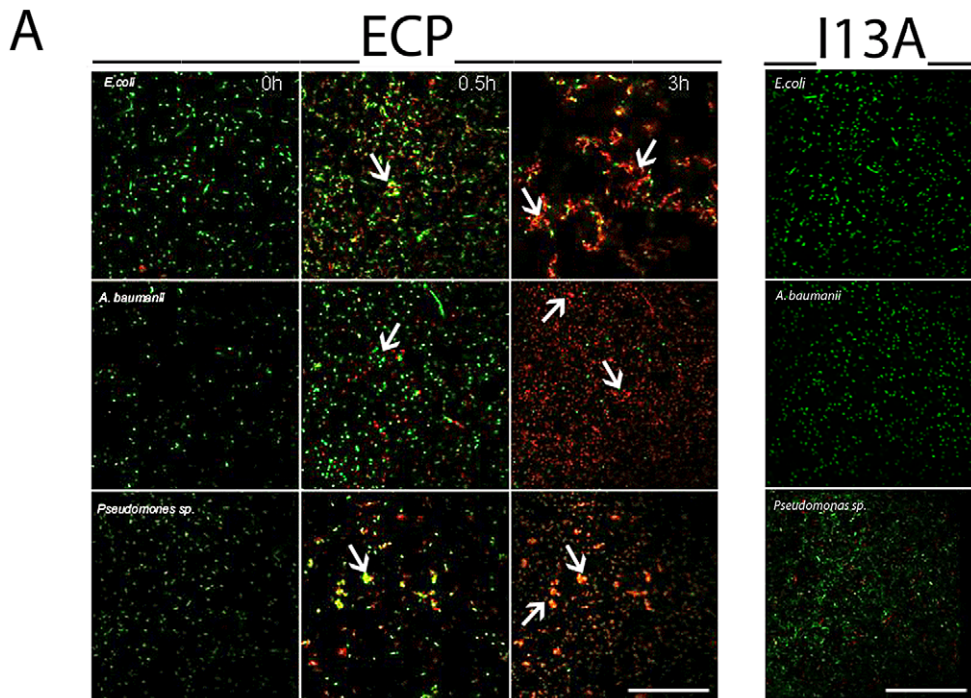


Figure 1. ECP but not I13A is able to agglutinate bacteria. (A) *E. coli*, *P. aeruginosa* and *A. baumanii* cells were incubated with 5 μ M of ECP or I13A mutant in microscopy plates during 4 h and stained with syto9 (live cells, green) and propidium iodide (dead cells, red). Images were taken at 0, 0.5 and 3 h using a Leica SP2 confocal microscopy as described in the Materials and Methods section. Scale bar represents 50 μ m. Arrows were depicted to show cell agglutination. Images depicted are representative from two independent experiments. (B) *E. coli* cells were incubated with 5 μ M of ECP or I13A mutant during 4 h and samples were analyzed using a FACSCalibur cytometer. FSC-H is the low-angle forward scattering, which is roughly proportional to the diameter of the cell and SSC-H is the orthogonal or side scattering, which is proportional to cell granularity or complexity. Agglutination is registered as an increase in both scattering measures. In all experiments cell cultures were grown at exponential phase ($OD_{600}=0.2$) and incubated with proteins in 10 mM sodium phosphate buffer, 100 mM NaCl, pH 7.4. The plots are representative of three independent experiments.

doi:10.1371/journal.ppat.1003005.g001

abolishes the cell agglutinating activity of ECP but also its bactericidal action.

Agglutination mediated by protein aggregation

Next, to address the question whether cell agglutination is consistently driven by protein aggregation at the bacteria surface, we incubated bacteria cultures with ECP and visualized the samples using confocal microscopy. Our results show that wtECP binds to the bacteria surface and a strong protein signal is registered at the aggregation zones (Figure 3A). On the contrary, though cell interaction is maintained for the I13A mutant, agglutination is observed neither in bacteria cell cultures nor in model membranes (Figures 3A and 3B). As expected, for model membranes we show that only wtECP is able to promote agglutination (Figure 3B). Therefore, we conclude that protein aggregation on the cellular surface is required for bacteria agglutination, which turns to be essential for the antimicrobial action. Agglutination is also observed in the presence of 20% plasma in a similar extent, suggesting that ECP agglutination is likely to take place in the physiological context (Supplementary Information Figure S3). As previously mentioned, ECP binding to bacteria is favored by interactions with the LPS outer membrane [35,41,47]. Consistently, we show here that LPS binding activity is lost for the I13A mutant, when compared with wtECP (Supplementary Information Figure S4).

In situ follow-up of amyloid aggregates

At this point however, the nature of the protein aggregates remained unknown. Thus, having previously shown that ECP is able to form amyloid-like aggregates *in vitro*, we decided to test if the observed aggregates have an amyloid-like structure using the amyloid-diagnostic dyes Thioflavin-T and Congo Red. When bacteria cultures are incubated with non-labeled wtECP, stained with ThT and visualized by total internal reflection fluorescence (TIRF) microscopy, we show that wtECP amyloid-like aggregates are located also at the cell surface (Figure 4A) similarly as what we observe for Alexa labeled wtECP (Figure 3A). Consistently, no staining is observed for non-incubated cultures and for the I13A mutant (Figure 4A). Moreover, upon bacteria incubation with wtECP, a red shift in the Congo Red spectrum is observed (Supplementary Information Figure S5A), revealing that the protein amyloid-like aggregation is triggered upon incubation with bacteria cultures.

Though ECP was previously shown to form amyloid-like aggregates *in vitro* only at low pH after a long incubation time (1–2 weeks), amyloid-like structures observed here are detected after only 4 hours of incubation. However, it is well known that some proteins can accelerate its aggregation kinetics in the presence of membrane-like environments [48–50]. Our results show that wtECP is able to form fibrillar-like aggregates on model membranes with an average size of 845 ± 150 nm (Figure 4B), comparable in size with the wtECP aggregates observed *in vitro* in the absence of lipid membranes (~ 150 nm) [28]. In fact, when tested for ThT binding, we observe aggregates with similar size

(Figure 4B). When wtECP is incubated with model membranes and tested for Congo Red binding, we obtain again a noticeable spectral shift (Supplementary Information Figure S5B). To complete these results we have also performed all the experiments detailed above using the I13A mutant and found it to be unable to form amyloid-like aggregates (Figure 4).

Conclusions

The results presented here for ECP reinforce the hypothesis that an amyloid-like aggregation process is taking place in the bacteria surface that drives bacteria cell agglutination, which is essential for the antimicrobial activity of the protein. In summary, after binding to the bacteria surface, a rearrangement of the protein could take place, exposing the hydrophobic N-terminal patch of the protein. Following, the aggregation process would start promoting the agglutination of the bacteria cells through the aggregation of the surface-attached protein molecules. The formation of aggregates on the bacteria surface will disrupt the lipopolysaccharide bilayer of Gram-negative cells exposing the internal cytoplasmatic membrane to the protein action, promoting the membrane disruption and eventually the bacteria killing.

Cell agglutinating activity provides a particularly appealing feature that may contribute to the clearance of bacteria at the infectious focus. In this sense, bacteria agglutination would prepare the field before host phagocytic cells enter in the scene [33]. However, despite the interest in the pharmaceutical industry to identify the structural determinants for bacteria cell agglutination, bibliography on that subject is scarce and only few agglutinating antimicrobial proteins are described in the literature. Excitingly, there may be other proteins and peptides with similar characteristics that also follow the proposed model. Hence, the agglutinating mechanism may represent a more generalized process that may derive in amyloid deposit formation at bacterial infection focuses.

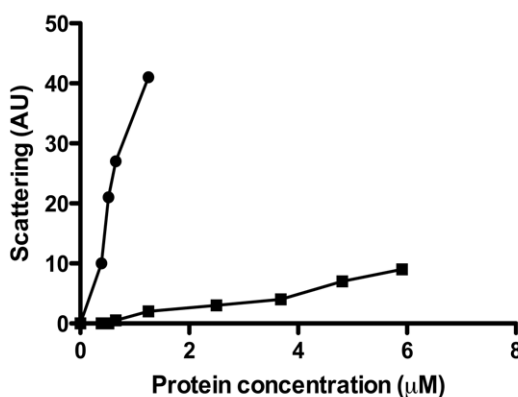
Besides, it has been reported that systematic exposure to inflammation may represent a risk factor on developing Alzheimer's disease [51,52] and other types of dementia [53]. Some studies have also demonstrated that the release of inflammatory mediators can also cause generalized cytotoxicity. In particular, ECP has been discovered to be cytotoxic [40,54] and neurotoxic, causing the Gordon phenomenon after injection intratechally in rabbits [55]. Therefore, our results suggest that the release of inflammatory mediators after infection (like AMPs) may either seed the aggregation processes in the brain and/or influence the membrane biophysical properties to trigger neurotoxicity and aggregation events.

Materials and Methods

MIC (Minimal Inhibitory Concentration) and MAC (Minimal Agglutination Concentration) determination

Antimicrobial activity was expressed as the MIC₁₀₀, defined as the lowest protein concentration that completely inhibits microbial growth. MIC of each protein was determined from two

A



B

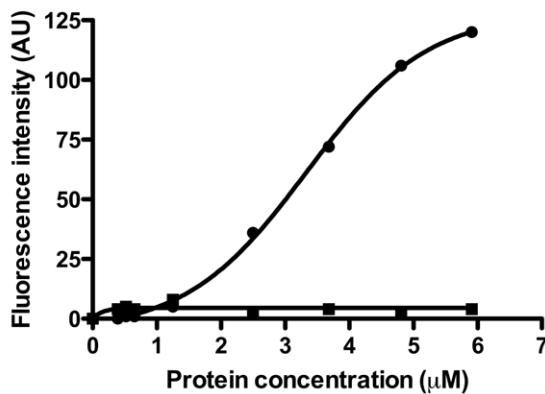


Figure 2. Liposome agglutination and leakage activity. wtECP (circles) and I13A mutant (squares) were incubated with liposomes and the agglutination (A) and leakage (B) were followed at increasing protein concentrations (1–6 μM). Agglutination was measured as light scattering (470 nm) at 90° from the beam source in a 10 mM Tris-HCl, 100 mM NaCl, pH 7.4 buffer and leakage was followed using the ANTS/DPX assay in the same buffer as described in the Materials and Methods section.

doi:10.1371/journal.ppat.1003005.g002

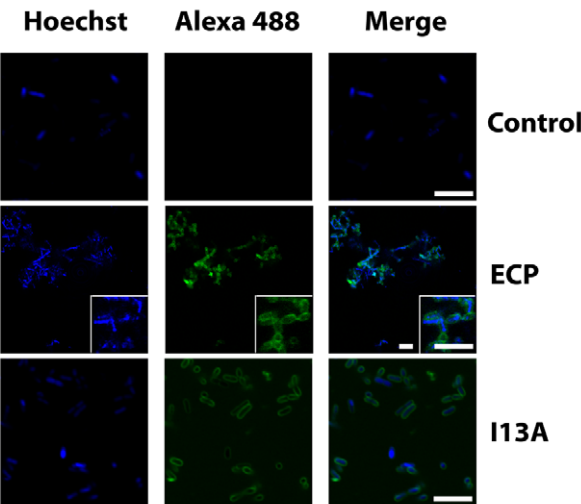
independent experiments performed in triplicate for each concentration. Bacteria were incubated at 37°C overnight in Mueller-Hinton II (MHII) broth and diluted to give approximately $5 \cdot 10^5$ CFU/mL. Bacterial suspension was incubated with proteins at various concentrations (0.1–5 μM) at 37°C for 4 h either in MHII or 10 mM sodium phosphate buffer, 100 mM NaCl, pH 7.4. Samples were plated onto Petri dishes and incubated at 37°C overnight.

For MAC determination, bacteria cells were grown at 37°C to mid-exponential phase ($\text{OD}_{600} = 0.6$), centrifuged at 5000 $\times g$ for 2 min, and resuspended in 10 mM sodium phosphate buffer, 100 mM NaCl, pH 7.4, in order to give an absorbance of 0.2 at 600 nm. A 200 μL aliquot of the bacterial suspension was incubated with proteins at various (0.1–10 μM) concentrations at 25°C for 4 h. Aggregation behavior was observed by visual inspection and minimal agglutinating concentration expressed as previously described [42].

Fluorescence-Assisted Cell Sorting (FACS) assay

Bacteria cells were grown at 37°C to mid-exponential phase ($\text{OD}_{600} = 0.6$), centrifuged at 5000 $\times g$ for 2 min, resuspended in 10 mM sodium phosphate buffer, 100 mM NaCl, pH 7.4 or the same buffer supplemented with 20% plasma to give a final

A



B

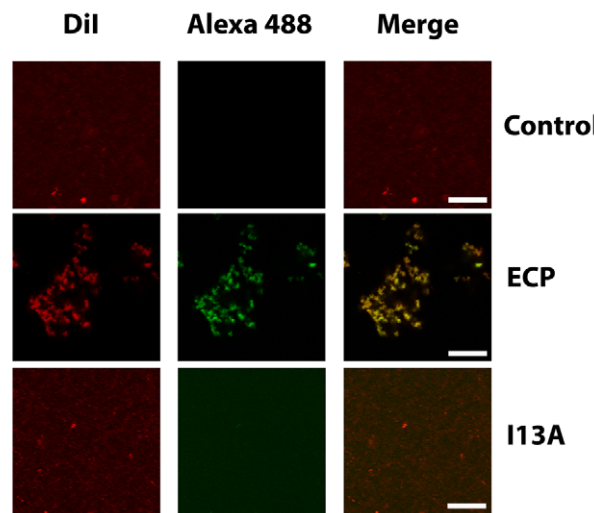


Figure 3. ECP and I13A mutant bind to the surface of bacteria and membranes. (A) *E. coli* bacteria cells stained with Hoechst (blue signal) were incubated with 5 μM of either wtECP or I13A mutant (both labeled with Alexa Fluor 488; green signal) for 4 h and visualized by confocal microscopy. In all experiments cell cultures were grown at exponential phase ($\text{OD}_{600} = 0.2$) and incubated with proteins in 10 mM sodium phosphate buffer, 100 mM NaCl, pH 7.4. (B) 500 μL of 200 μM LUV liposomes stained with Dil (red signal) were incubated with 5 μM of either wtECP or I13A mutant (both labeled with Alexa Fluor 488; green signal) for 4 h and visualized using a Leica SP2 confocal microscope. Scale bars are 5 μm length in all images and insight captions. Images depicted are representative from two independent experiments.

doi:10.1371/journal.ppat.1003005.g003

$\text{OD}_{600} = 0.2$ and preincubated for 20 min. A 500 μL aliquot of the bacterial suspension was incubated with 5 μM of wtECP or I13A mutant during 4 h. After incubation, 25000 cells were subjected to FACS analysis using a FACSCalibur cytometer (BD Biosciences, New Jersey) and a dot-plot was generated by representing the low-angle forward scattering (FSC-H) in the x-axis and the side scattering (SSC-H) in the y-axis to analyze the size and complexity of the cell cultures. Results were analyzed using FlowJo (Tree Star, Ashland, OR).

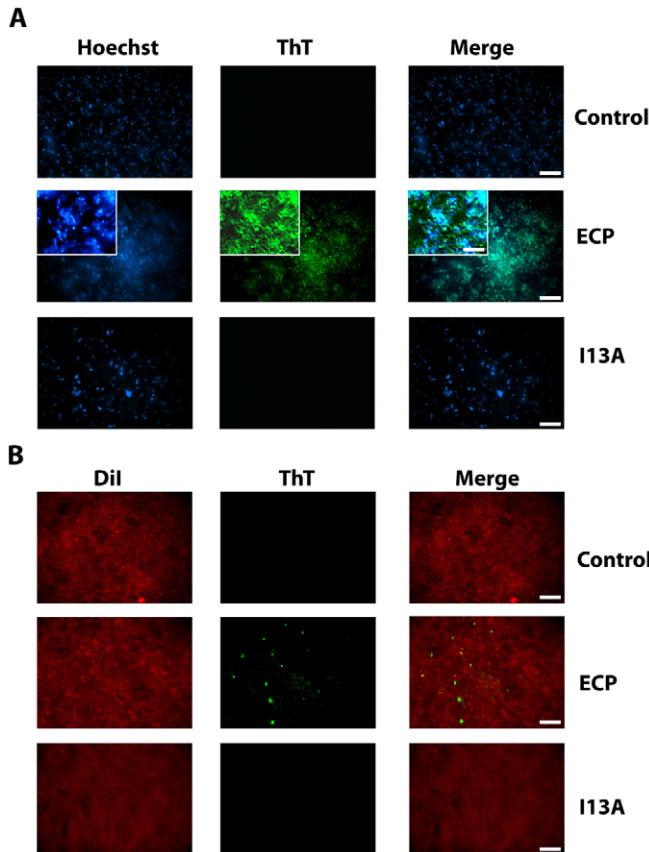


Figure 4. ECP but not I13A form amyloid-like aggregates on the surface of bacteria and membranes. (A) *E. coli* bacteria cells stained with Hoechst (blue signal) were incubated with unlabeled wtECP or I13A mutant for 4 h, stained with ThT (green signal) and visualized by TIRF microscopy. In all experiments cell cultures were grown at exponential phase ($OD_{600}=0.2$) and incubated with proteins in 10 mM sodium phosphate buffer, 100 mM NaCl, pH 7.4. (B) Planar lipid bilayers prepared as described in the Materials and Methods section (stained with Dil; red signal) were incubated with 5 μ M of either unlabeled wtECP or I13A mutant for 4 h, stained with 25 μ M ThT (green signal) and visualized using a Olympus Fluoview 1000 TIRF microscope. Scale bar represents 20 μ m (5 μ m in the insight caption). Images depicted are representative from two independent experiments.

doi:10.1371/journal.ppat.1003005.g004

Bacteria viability assay

Bacteria viability assays were performed as described before [39]. Briefly, bacteria were incubated in 10 mM sodium phosphate buffer, 100 mM NaCl, pH 7.4 with 5 μ M of wtECP or I13A mutant and then stained using a syto 9/propidium iodide 1:1 mixture. The viability kinetics were monitored using a Cary Eclipse Spectrofluorimeter (Varian Inc., Palo Alto, CA, USA). To calculate bacterial viability, the signal in the range 510–540 nm was integrated to obtain the syto 9 signal (live bacteria) and from 620–650 nm to obtain the propidium iodide signal (dead bacteria). Then, the percentage of live bacteria was represented as a function of time.

Liposome agglutination and leakage assay

The ANTS/DPX liposome leakage fluorescence assay was performed as previously described [56]. Briefly, a unique population of LUVs of DOPC/DOPG (3:2 molar ratio) lipids was obtained containing 12.5 mM ANTS, 45 mM DPX, 20 mM NaCl, and 10 mM Tris/HCl, pH 7.4. The ANTS/DPX liposome suspension was diluted to 30 μ M concentration and incubated at 25°C in the presence of wtECP or I13A mutant. Leakage activity was followed by monitoring the increase of the fluorescence at 535 nm.

For liposome agglutination, 200 μ M LUV liposomes were incubated in 10 mM phosphate buffer, pH 7.4, containing 5 to 100 mM NaCl, in the presence of 5 μ M wtECP or I13A mutant

and the scattering signal at 470 nm was collected at 90° from the beam source using a Cary Eclipse Spectrofluorimeter (Varian Inc., Palo Alto, CA, USA) [57].

Confocal microscopy

Experiments were carried out in 35 cm² plates with a glass coverslip. For phospholipid membranes, 500 μ l of 200 μ M LUV liposomes (prepared as described in Supplementary Information) were incubated with 5 μ M wtECP or I13A mutant for 4 h in 10 mM sodium phosphate buffer, 100 mM NaCl, pH 7.4. For bacteria, 500 μ l of *E. coli* cells ($OD_{600}=0.2$) were incubated with 5 μ M wtECP or I13A mutant for 4 h in 10 mM sodium phosphate buffer, 100 mM NaCl, pH 7.4. RNase A was used always as a negative control. Samples of both liposomes and bacteria were imaged using a laser scanning confocal microscope (Olympus Fluoview 1000 equipped with a UPlansApo 60 \times objective in 1.4 oil immersion objective, United Kingdom). wtECP and I13A mutant labeled with Alexa Fluor 488 were excited using a 488-nm argon laser (515–540 nm emission collected) and Vibrant DiI was excited using an orange diode (588–715 nm emission collected).

TIRF microscopy

To study the interaction of proteins with lipid membranes, planar supported lipid bilayers were used (Supplementary

Information). When using bacteria, glass coverslips were previously treated with 0.1% poly-L-lysine to ensure that samples will adhere to the surface. 500 μ l of *E. coli* cells ($OD_{600}=0.2$) were incubated with 5 μ M wtECP or I13A mutant for 4 h and then transferred to poly-L-lysine treated microscopy plates and incubated for 15 minutes. To remove unattached cells, plates were washed twice with 10 mM sodium phosphate, 100 mM NaCl, pH 7.4 buffer. RNase A was used always as a negative control. Images were captured using a laser scanning confocal microscope (Olympus Fluoview 1000 equipped with a PlanApo 60 \times TIRF objective in 1.4 oil immersion objective, United Kingdom) using the same conditions as described for confocal microscopy experiments. Thioflavin T (ThT) was used to detect amyloid aggregates. In this case, samples were incubated for 4 h with unlabeled proteins as described before and then incubated with ThT at 25 μ M final concentration for 15 minutes. Then, plates were washed twice with 10 mM sodium phosphate, 100 mM NaCl buffer, pH 7.4 to remove unattached cells and ThT excess.

Supporting Information

Figure S1 Bacteria agglutination mediated by wtECP and the I13A mutant. *E. coli* bacteria cells were grown at exponential phase ($OD_{600}=0.2$) and incubated with 0.5 μ M wtECP (A) or I13A (B) in 10 mM phosphate buffer, 100 mM NaCl, pH 7.5 for 4 h. Images were taken using a Leica magnificator. wtECP incubated bacteria samples were also observed under 40 \times (C) and 100 \times (D) magnification to reveal more details on bacteria aggregates. Images were taken using a Leica optical microscope.

(TIF)

Figure S2 Liposome agglutination mediated by wtECP and I13A mutant at increasing ionic strength. Liposomes prepared as described in the Materials and Methods section were incubated with increasing concentrations of wtECP (circles) or I13A mutant (squares) at 5 mM (A), 50 mM (B) and 100 mM (C) NaCl in a 10 mM phosphate buffer, pH 7.5. The formation of liposome aggregates was followed as an increase in the light scattering signal at 90° from the beam.

(TIF)

Figure S3 ECP is able to agglutinate bacteria cells in plasma. *E. coli* cells were incubated with 5 μ M of ECP during 4 h and samples were analyzed using a FACSCalibur cytometer. FSC-H is the low-angle forward scattering, which is roughly proportional to the diameter of the cell and SSC-H is the orthogonal or side scattering, which is proportional to cell

References

1. Otvos L, Jr. (2005) Antibacterial peptides and proteins with multiple cellular targets. *J Pept Sci* 11: 697–706.
2. Yount NY, Bayer AS, Xiong YQ, Yeaman MR (2006) Advances in antimicrobial peptide immunobiology. *Biopolymers* 84: 435–458.
3. Zasloff M (2002) Antimicrobial peptides of multicellular organisms. *Nature* 415: 389–395.
4. Hancock RE, Sahl HG (2006) Antimicrobial and host-defense peptides as new anti-infective therapeutic strategies. *Nat Biotechnol* 24: 1551–1557.
5. Zhang L, Falla TJ (2010) Potential therapeutic application of host defense peptides. *Methods Mol Biol* 618: 303–327.
6. Brogden KA (2005) Antimicrobial peptides: pore formers or metabolic inhibitors in bacteria? *Nat Rev Microbiol* 3: 238–250.
7. Gotter LM, Ramamoorthy A (2009) Structure, membrane orientation, mechanism, and function of pexiganan—a highly potent antimicrobial peptide designed from magainin. *Biochim Biophys Acta* 1788: 1680–1686.
8. Marsh EN, Buer BC, Ramamoorthy A (2009) Fluorine—a new element in the design of membrane-active peptides. *Mol Biosyst* 5: 1143–1147.
9. Ramamoorthy A (2009) Beyond NMR spectra of antimicrobial peptides: dynamical images at atomic resolution and functional insights. *Solid State Nucl Magn Reson* 35: 201–207.
10. Thennarasu S, Huang R, Lee DK, Yang P, Maloy L, et al. (2010) Limiting an antimicrobial peptide to the lipid-water interface enhances its bacterial membrane selectivity: a case study of MSI-367. *Biochemistry* 49: 10595–10605.
11. Pulido D, Nogues MV, Boix E, Torrent M (2012) Lipopolysaccharide neutralization by antimicrobial peptides: a gambit in the innate host defense strategy. *J Innate Immun* 4: 327–336.
12. Torrent M, Nogues MV, Boix E (2012) Discovering new *in silico* tools for antimicrobial Peptide prediction. *Curr Drug Targets* 13: 1148–1157.
13. Wimley WC (2010) Describing the mechanism of antimicrobial peptide action with the interfacial activity model. *ACS Chem Biol* 5: 905–917.
14. Nguyen LT, Haney EF, Vogel HJ (2011) The expanding scope of antimicrobial peptide structures and their modes of action. *Trends Biotechnol* 29: 464–472.
15. Butterfield SM, Lashuel HA (2010) Amyloidogenic protein-membrane interactions: mechanistic insight from model systems. *Angew Chem Int Ed Engl* 49: 5628–5654.

granularity or complexity. Agglutination is registered as an increase in both scattering measures. In all experiments, cell cultures were grown at exponential phase ($OD_{600}=0.2$) and incubated with proteins in 20% plasma diluted in 10 mM sodium phosphate buffer, 100 mM NaCl, pH 7.5. The plots are representative of three independent experiments. (TIF)

Figure S4 wtECP and I13A mutant binding to bacteria

LPS. LPS were incubated with increasing concentrations of wtECP (circles) or I13A mutant (squares) in a 10 mM phosphate buffer, 100 mM NaCl, pH 7.5. Binding to bacteria LPS was registered as a fluorescence increase of the BODIPY-cadaverine reporter as described in the Materials and Methods section. The occupancy factor denotes the decrease of the LPS-bound dye fraction after protein addition.

(TIF)

Figure S5 Protein aggregates bind to Congo Red dye.

(A) *E. coli* (circles) and *P. aeruginosa* (triangles) bacteria cells were incubated 4 h with wtECP and assayed for Congo Red binding as described in the Materials and Methods section. **(B)** Liposomes at 10 μ M (black circles), 200 μ M (grey circles) and 1 mM (white squares) lipid concentration were incubated with wtECP and assayed for Congo Red binding as described in the Materials and Methods section. Congo Red differential spectra were obtained by subtracting both the signal corresponding to the protein and the lipid/bacteria in the presence of the dye. The vertical line at 480 nm represents the spectrum of Congo Red alone. Incubation of I13A mutant with both bacteria and membranes did not display any significant spectral shift.

(TIF)

Protocol S1 This file contains additional details for the Materials and Methods section.

(DOCX)

Acknowledgments

Microscopy experiments were carried at the Servei de Microscòpia (UAB) and fluorescence measurements at Servei d'Anàlisi i Fotodocumentació (UAB). We thank Natalia Sánchez de Groot for her assistance in the FACS analysis.

Author Contributions

Conceived and designed the experiments: MT EB. Performed the experiments: MT DP. Analyzed the data: MT DP MVN EB. Contributed reagents/materials/analysis tools: MVN EB. Wrote the paper: MT EB.

16. Mahalka AK, Kinnunen PK (2009) Binding of amphipathic alpha-helical antimicrobial peptides to lipid membranes: lessons from temporins B and L. *Biochim Biophys Acta* 1788: 1600–1609.
17. Kagan BL, Jang H, Capone R, Teran Arce F, Ramachandran S, et al. (2011) Antimicrobial Properties of Amyloid Peptides. *Mol Pharm* 9:708–717.
18. Brender JR, Durr UH, Heyl D, Budarapu MB, Ramamoorthy A (2007) Membrane fragmentation by an amyloidogenic fragment of human Islet Amyloid Polypeptide detected by solid-state NMR spectroscopy of membrane nanotubes. *Biochim Biophys Acta* 1768: 2026–2029.
19. Brender JR, Hartman K, Gottler LM, Cavit ME, Youngstrom DW, et al. (2009) Helical conformation of the SEVI precursor peptide PAP248–286, a dramatic enhancer of HIV infectivity, promotes lipid aggregation and fusion. *Biophys J* 97: 2474–2483.
20. Brender JR, Hartman K, Reid KR, Kennedy RT, Ramamoorthy A (2008) A single mutation in the nonamyloidogenic region of islet amyloid polypeptide greatly reduces toxicity. *Biochemistry* 47: 12680–12688.
21. Brender JR, Lee EL, Cavit MA, Gafni A, Steel DG, et al. (2008) Amyloid fiber formation and membrane disruption are separate processes localized in two distinct regions of IAPP, the type-2-diabetes-related peptide. *J Am Chem Soc* 130: 6424–6429.
22. Nanga RP, Brender JR, Vivekanandan S, Popovych N, Ramamoorthy A (2009) NMR structure in a membrane environment reveals putative amyloidogenic regions of the SEVI precursor peptide PAP(248–286). *J Am Chem Soc* 131: 17972–17979.
23. Nanga RP, Brender JR, Xu J, Hartman K, Subramanian V, et al. (2009) Three-dimensional structure and orientation of rat islet amyloid polypeptide protein in a membrane environment by solution NMR spectroscopy. *J Am Chem Soc* 131: 8252–8261.
24. Popovych N, Brender JR, Soong R, Vivekanandan S, Hartman K, et al. (2012) Site specific interaction of the polyphenol EGCG with the SEVI amyloid precursor peptide PAP(248–286). *J Phys Chem B* 116: 3650–3658.
25. Jelinek R, Kolusheva S (2005) Membrane interactions of host-defense peptides studied in model systems. *Curr Protein Pept Sci* 6: 103–114.
26. Tang M, Hong M (2009) Structure and mechanism of beta-hairpin antimicrobial peptides in lipid bilayers from solid-state NMR spectroscopy. *Mol Biosyst* 5: 317–322.
27. Torrent M, Valle J, Nogues MV, Boix E, Andreu D (2011) The generation of antimicrobial peptide activity: a trade-off between charge and aggregation? *Angew Chem Int Ed Engl* 50: 10686–10689.
28. Torrent M, Odorizzi F, Nogues MV, Boix E (2010) Eosinophil cationic protein aggregation: identification of an N-terminus amyloid prone region. *Biomacromolecules* 11: 1983–1990.
29. Jang H, Arce FT, Mustata M, Ramachandran S, Capone R, et al. (2011) Antimicrobial protegrin-1 forms amyloid-like fibrils with rapid kinetics suggesting a functional link. *Biophys J* 100: 1775–1783.
30. Soscia SJ, Kirby JE, Washicosky KJ, Tucker SM, Ingelsson M, et al. (2010) The Alzheimer's disease-associated amyloid beta-protein is an antimicrobial peptide. *PLoS One* 5: e9505.
31. Harris F, Dennison SR, Phoenix DA (2012) Aberrant action of amyloidogenic host defense peptides: a new paradigm to investigate neurodegenerative disorders? *FASEB J* 26: 1776–1781.
32. Torrent M, Andreu D, Nogues VM, Boix E (2011) Connecting peptide physicochemical and antimicrobial properties by a rational prediction model. *PLoS One* 6: e16968.
33. Gorr SU, Sotsky JB, Shular AP, Demuth DR (2008) Design of bacteria-agglutinating peptides derived from parotid secretory protein, a member of the bactericidal/permeability increasing-like protein family. *Peptides* 29: 2118–2127.
34. Van Nieuw Amerongen A, Bolscher JG, Veerman EC (2004) Salivary proteins: protective and diagnostic value in cariology? *Caries Res* 38: 247–253.
35. Pulido D, Moussaoui M, Andreu D, Nogues MV, Torrent M, et al. (2012) Antimicrobial Action and Cell Agglutination by Eosinophil Cationic Protein Is Modulated by the Cell Wall Lipopolysaccharide Structure. *Antimicrob Agents Chemother* 56: 2378–2385.
36. Boix E, Torrent M, Sánchez D, Nogués MV (2008) The Antipathogen Activities of Eosinophil Cationic Protein. *Current Pharm Biotec* 9: 141–152.
37. Venge P, Byström J, Carlson M, Hakansson L, Karawaczky M, et al. (1999) Eosinophil cationic protein (ECP): molecular and biological properties and the use of ECP as a marker of eosinophil activation in disease. *Clin Exp Allergy* 29: 1172–1186.
38. Boix E, Salazar VA, Torrent M, Pulido D, Nogués MV, et al. (2012) Structural determinants of the eosinophil cationic protein antimicrobial activity. *Biol Chem* 393: 801–815.
39. Torrent M, Badia M, Moussaoui M, Sanchez D, Nogués MV, et al. (2010) Comparison of human RNase 3 and RNase 7 bactericidal action at the Gram-negative and Gram-positive bacterial cell wall. *FEBS J* 277: 1713–1725.
40. Navarro S, Aleu J, Jimenez M, Boix E, Cuchillo CM, et al. (2008) The cytotoxicity of eosinophil cationic protein/ribonuclease 3 on eukaryotic cell lines takes place through its aggregation on the cell membrane. *Cell Mol Life Sci* 65: 324–337.
41. Torrent M, Navarro S, Moussaoui M, Nogués MV, Boix E (2008) Eosinophil cationic protein high-affinity binding to bacteria-wall lipopolysaccharides and peptidoglycans. *Biochemistry* 47: 3544–3555.
42. Torrent M, Pulido D, de la Torre BG, García-Mayoral MF, Nogués MV, et al. (2011) Refining the eosinophil cationic protein antibacterial pharmacophore by rational structure minimization. *J Med Chem* 54: 5237–5244.
43. Sanchez D, Moussaoui M, Carreras E, Torrent M, Nogués V, et al. (2011) Mapping the eosinophil cationic protein antimicrobial activity by chemical and enzymatic cleavage. *Biochimie* 93: 331–338.
44. Torrent M, Di Tommaso P, Pulido D, Nogués MV, Notredame C, et al. (2012) AMPA: an automated web server for prediction of protein antimicrobial regions. *Bioinformatics* 28: 130–131.
45. Torrent M, Nogués VM, Boix E (2009) A theoretical approach to spot active regions in antimicrobial proteins. *BMC Bioinformatics* 10: 373.
46. Torrent M, de la Torre BG, Nogués VM, Andreu D, Boix E (2009) Bactericidal and membrane disruption activities of the eosinophil cationic protein are largely retained in an N-terminal fragment. *Biochim J* 421: 425–434.
47. Torrent M, Nogués MV, Boix E (2011) Eosinophil cationic protein (ECP) can bind heparin and other glycosaminoglycans through its RNase active site. *J Mol Recognit* 24: 90–100.
48. Kayed R, Sokolov Y, Edmonds B, McIntire TM, Milton SC, et al. (2004) Permeabilization of lipid bilayers is a common conformation-dependent activity of soluble amyloid oligomers in protein misfolding diseases. *J Biol Chem* 279: 46363–46366.
49. Ambroggio EE, Kim DH, Sepovic F, Barrow CJ, Barnham KJ, et al. (2005) Surface behavior and lipid interaction of Alzheimer beta-amyloid peptide 1–42: a membrane-disrupting peptide. *Biophys J* 88: 2706–2713.
50. Auvynet C, El Amri C, Lacombe C, Bruston F, Bourdais J, et al. (2008) Structural requirements for antimicrobial versus chemoattractant activities for dermaseptin S9. *FEBS J* 275: 4134–4151.
51. Krstic D, Madhusudan A, Doehner J, Vogel P, Notter T, et al. (2012) Systemic immune challenges trigger and drive Alzheimer-like neuropathology in mice. *J Neuroinflammation* 9: 151.
52. Miklossy J (2011) Emerging roles of pathogens in Alzheimer disease. *Expert Rev Mol Med* 13: e30.
53. Almeida OP, Lautenschlager NT (2005) Dementia associated with infectious diseases. *Int Psychogeriatr* 17 Suppl 1: S65–77.
54. Navarro S, Boix E, Cuchillo CM, Nogués MV (2010) Eosinophil-induced neurotoxicity: the role of eosinophil cationic protein/RNase 3. *J Neuroimmunol* 227: 60–70.
55. Fredens K, Dahl R, Venge P (1982) The Gordon phenomenon induced by the eosinophil cationic protein and eosinophil protein X. *J Allergy Clin Immunol* 70: 361–366.
56. Torrent M, Cuyas E, Carreras E, Navarro S, Lopez O, et al. (2007) Topography studies on the membrane interaction mechanism of the eosinophil cationic protein. *Biochemistry* 46: 720–733.
57. Torrent M, Sanchez D, Buzon V, Nogués MV, Cladera J, et al. (2009) Comparison of the membrane interaction mechanism of two antimicrobial RNases: RNase 3/ECP and RNase 7. *Biochim Biophys Acta* 1788: 1116–1125.